Hydrol. Earth Syst. Sci., 16, 2567–2583, 2012
www.hydrol-earth-syst-sci.net/16/2567/2012/
doi:10.5194/hess-16-2567-2012

Hydrology and Earth System Sciences

Improving evapotranspiration in a land surface model using biophysical variables derived from MSG/SEVIRI satellite

N. Ghilain[1], A. Arboleda[1], G. Sepulcre-Cantò[1,*], O. Batelaan[2,3], J. Ardö[4], and F. Gellens-Meulenberghs[1]

[1]Royal Meteorological Institute of Belgium, Avenue circulaire 3, 1180 Brussels, Belgium
[2]Dept. of Hydrology and Hydraulic Engineering, Vrije Universiteit Brussel, Pleinlaan 2, 1050 Brussels, Belgium
[3]Dept. Earth and Environmental Sciences, Katholieke Universiteit Leuven, Celestijnenlaan 200E, 3001 Heverlee, Belgium
[4]Dept. Physical Geography and Ecosystems Analysis, Lund University, Sölvegatan 12, 223 62 Lund, Sweden
[*]now at: Institute for Environment and Sustainability, Joint Research Center, Ispra, Italy

Correspondence to: N. Ghilain (nicolas.ghilain@meteo.be)

Received: 29 September 2011 – Published in Hydrol. Earth Syst. Sci. Discuss.: 14 October 2011
Revised: 29 June 2012 – Accepted: 5 July 2012 – Published: 8 August 2012

Abstract. Monitoring evapotranspiration over land is highly dependent on the surface state and vegetation dynamics. Data from spaceborn platforms are desirable to complement estimations from land surface models. The success of daily evapotranspiration monitoring at continental scale relies on the availability, quality and continuity of such data. The biophysical variables derived from SEVIRI on board the geostationary satellite Meteosat Second Generation (MSG) and distributed by the Satellite Application Facility on Land surface Analysis (LSA-SAF) are particularly interesting for such applications, as they aimed at providing continuous and consistent daily time series in near-real time over Africa, Europe and South America. In this paper, we compare them to monthly vegetation parameters from a database commonly used in numerical weather predictions (ECOCLIMAP-I), showing the benefits of the new daily products in detecting the spatial and temporal (seasonal and inter-annual) variability of the vegetation, especially relevant over Africa. We propose a method to handle Leaf Area Index (LAI) and Fractional Vegetation Cover (FVC) products for evapotranspiration monitoring with a land surface model at 3–5 km spatial resolution. The method is conceived to be applicable for near-real time processes at continental scale and relies on the use of a land cover map. We assess the impact of using LSA-SAF biophysical variables compared to ECOCLIMAP-I on evapotranspiration estimated by the land surface model H-TESSEL. Comparison with in-situ observations in Europe and Africa shows an improved estimation of the evapotranspiration, especially in semi-arid climates. Finally, the impact on the land surface modelled evapotranspiration is compared over a north–south transect with a large gradient of vegetation and climate in Western Africa using LSA-SAF radiation forcing derived from remote sensing. Differences are highlighted. An evaluation against remote sensing derived land surface temperature shows an improvement of the evapotranspiration simulations.

1 Introduction

In the past decades, an increasing number of models were developed to monitor evapotranspiration (ET) at different scales using remote sensing measurements. Simple empirical or statistical methods to fully detailed physical models have been developed, using a wealth of information provided by various satellites (e.g. Courault et al., 2005; Kalma et al., 2008; Li et al., 2009). In all methods, vegetation has been recognized to be a cornerstone of the evapotranspiration process since plants are the main medium for exchange of water between the soil and the atmosphere. In particular, land surface models are widely used for meteorological and climate studies. They are based on a conceptual and semi-empirical description of, respectively, the physical and physiological processes of heat and water exchanges between soil, plants and atmosphere media. Information usually needed for land surface models is 1) the exact coverage of plant functional types (PFT) (Bonan et al., 2002), information given by a land cover map, 2) the state of the vegetation development,

mostly given by the variable Leaf Area Index (LAI). While most of those models require explicit external information on the vegetation status (e.g. Balsamo et al., 2009; Noilhan and Planton, 1989), a new generation of models considers it as a new model variable (e.g. Jarlan et al., 2008; Gibelin et al., 2006; Blyth et al., 2006). But, for both model classes, information on vegetation status is highly relevant. For the first class, it is necessary information to provide. For the second one, it is recommended for updating the model forecasts (e.g. Jarlan et al., 2008; Albergel et al., 2010), or at least evaluate their output (e.g. Brut et al., 2009). Past studies have used variety of land surface models or crop growth models and different vegetation products issued from remote sensing (e.g. Dorigo et al., 2006). In this way, the use of remote sensing vegetation indices has revealed an improved forecast of surface variables.

Different exploitations have become possible along with the ever growing length of time series available from remote sensing. Early usage of the vegetation indices in soil-vegetation-atmosphere transfer (SVAT) models focused on a mean vegetation status by plant type throughout a year. New available long time series and reprocessing capabilities have given rise to vegetation databases, that include a mean monthly or weekly evolution of vegetation parameters, PFT and geographically dependent (e.g. ECOCLIMAP). Those two approaches have been widely used for operational purposes (e.g. van den Hurk et al., 2000, 2003) for practical reasons: easy to handle, not dependent on necessary incoming information from an external source, and hence on timeliness. However, the direct use of remote sensing time series is an important step towards a closer monitoring of the land surface, because it captures better both spatial and temporal variations including intra-species and inter-annual variability. For long-term monitoring of ET, it is necessary to capture the inter-annual variability of the vegetation state signal, which can be caused, for example, by a different date of budbreak for deciduous forests, harvest timing shifts (Cooley et al., 2005), rain occurence in semi-arid areas where the vegetation growth is driven by the hydrological regime, or by land re-allocation or fires. For the short term monitoring, at a daily time scale, poor time sampling of the vegetation phenology can have a negative impact on ET, especially during the rapid development stage of the canopy (e.g. Sepulcre-Cantó et al., 2012). Moreover, even if the classification in ecosystems of ECOCLIMAP-I is quite fine, the assumption of equal properties across different spatial scales for one ecosystem is an oversimplification of the problem.

Previous efforts have been carried out mainly using time series from polar orbiters (e.g. Albergel et al., 2010; Rodell et al., 2004). However, most of those studies focus on assimilation in a reanalysis mode, and cannot be used for a near-real time monitoring of the evapotranspiration. Recently, the EUMETSAT Land Surface Analysis Satellite Application Facility (LSA-SAF) developed a coordinated service in the area of remote sensing of the land surface and proposes products based on the geosynchronous MSG satellites (http://landsaf.meteo.pt) (Trigo et al., 2011). Among these products, remotely sensed biophysical parameter products, i.e. leaf area index, LSA-SAF LAI, and fractional vegetation cover (Fveg), LSA-SAF FVC, are delivered daily at the spatial resolution of the SEVIRI instrument on board MSG (LSA-SAF PUM VEGA, 2008) 3.1 km sub-satellite, and have been available since 2007. This study is done in the framework of land surface modelling for the purpose of ET monitoring at MSG/SEVIRI spatial resolution. It focuses on the applicability and gain of using biophysical variables issued from geostationary satellites, compared to monthly variables provided by databases.

In this paper, we demonstrate the advantages of using LSA-SAF biophysical variables. We compare them to those from ECOCLIMAP-I, and describe a method to use them in a land surface model at the same spatial resolution. A set of validation results over Europe and Africa and an example of application over West Africa further evaluated by comparison with complementary remote sensing data are presented.

In Sect. 2, we give a short description of the material for this study, which consists of a land surface model, the vegetation database used (ECOCLIMAP-I), and the LSA-SAF biophysical variables. In Sect. 3, we present a method to use the LSA-SAF biophysical variables in the land surface model in view of operational implementation. In Sect. 4, we compare the new vegetation dataset to ECOCLIMAP-I, highlighting its advantage. We analyze its characteristics and deduce a practical estimation mean to obtain robust estimates of biophysical variables. Then we evaluate the impact of using the new vegetation dataset on the modelled evapotranspiration against in-situ observations in Europe and Africa. Lastly, different aspects of the methodology and its application are discussed and conclusions from this work are outlined.

2 Material

2.1 The land surface model

The land surface model is based on H-TESSEL, the ECMWF land surface model (Beljaars and Viterbo, 1994; Viterbo and Beljaars, 1995; van den Hurk et al., 2000; Balsamo et al., 2009). It follows a bulk resistance formulation for the estimation of the surface turbulent fluxes, with two resistances modulating the variation of the sensible and latent heat fluxes. The aerodynamical resistance accounts for the turbulence generated by air temperature or wind gradient, while the stomatal resistance includes the influence of vapor pressure deficit, fraction of absorbed energy and soil water availability on the opening of the leaves stomata via a simple parameterization (van den Hurk et al., 2000). In addition, vertical distribution of moisture and temperature in the soil is modeled as a solution to diffusion equations. Direct evaporation from interception is modelled.

The needed forcing of this model consists of short and long-wave radiation reaching the land surface, surface albedo, wind speed, air temperature, air humidity and precipitation. In this model, the spatial unit for the energy balance assessment is divided into different tiles, associated with PFTs. The estimation of the surface fluxes is performed for each PFT before averaging over the spatial unit. The formulation uses parameters describing the vegetation state for each PFT separately: LAI, Fveg, roughness lengths, a minimum stomatal resistance, and the vertical distribution of the roots in the soil. The PFT classes have been changed from the original formulation of H-TESSEL to match the classification of ECOCLIMAP-I (Ghilain et al., 2011) and the model parameters have been calibrated.

The land surface model can be used at different spatial scales from a single point simulation using as input local measurements up to coarse grids used by global circulation models. In this paper, the model is applied at meso-scale and investigates the utility of the LSA-SAF biophysical variables. We therefore work in the MSG/SEVIRI grid, with a pixel as the basic model spatial unit.

The radiative terms used here are provided by the LSA-SAF: the downward surface short-wave (LSA-SAF DSSF) the long-wave fluxes (LSA-SAF DSLF) (Geiger et al., 2008a; Ineichen et al., 2009), and the surface albedo (LSA-SAF AL) (Geiger et al., 2008b; Carrer et al., 2010). LSA-SAF DSSF and DSLF are available half-hourly, while surface albedo is produced daily.

Meteorological forcing is provided by the Global Circulation Model re-analyses ERA-Interim (Simmons et al., 2006). The spatial resolution available is 0.5°and temporal sampling is 3 h. Meteorological forcing is linearly interpolated in time to half-hourly values. Tri-hourly precipitation rates are distributed equally for each 30 min step. If radiative forcing is missing, ERA-Interim is used to fill the gaps.

Complementary information on vegetation is needed: a land cover map and biophysical variables. Since each pixel can be composed of different PFTs, biophysical parameters must be known for each PFT inside the pixel, as well as the exact percentage that the PFTs occupy. The land surface model outputs an ET estimate each 30 min.

2.2 The ECOCLIMAP-I vegetation database

ECOCLIMAP-I (Masson et al., 2003; Champeaux et al., 2005) is a land cover map at 1 km resolution. In addition, it provides a vegetation parameterization for use in SVAT models in the form of a synthetic global vegetation database (http://www.cnrm.meteo.fr/gmme/PROJETS/ECOCLIMAP/pageecoclimap.htm, 2006). It is widely used by numerical weather prediction models in European countries (e.g. ALADIN International Team, 1997); furthermore, it is also used for inter-comparison of land surface models in Western Africa (Boone et al., 2009; Grippa et al., 2011), and in specific applications of H-TESSEL (Wipfler et al., 2011). Mixed ecosystems are decomposed into PFTs (defined in Table 1) and each PFT is associated with a 10 day or monthly varying set of biophysical variables (LAI, Fveg, roughness lengths) averaged spatially over all the grid cells occupied by the concerned ecosystem. ECOCLIMAP-I is used as in Ghilain et al. (2011).

The ecosystems are decomposed into PFTs compatible with the vegetation parameterization of the model, and the land cover map obtained at 1 km is projected onto the coarser model grid. The land cover map obtained gives the 5 dominant PFTs and their contribution to a satellite pixel. But, since one PFT can result from the combination of several ecosystems, LAI for each PFT is computed as the weighted mean contribution of the involved ecosystem's LAI. Monthly LAI maps at the satellite resolution are then created.

2.3 The LSA-SAF vegetation products

LSA-SAF LAI and FVC products (García-Haro et al., 2005a) are derived from MSG/SEVIRI using a two components Spectral Mixture Analysis method (García-Haro et al., 2005b; Verger et al., 2009). LSA-SAF operational center generates both variables daily, based on the past 5-days estimations, at the sensor spatial resolution. Retrieval uncertainty as well as a quality flag indicating the quality and reason for possible no production (e.g. snow, traces of snow, traces of inland water) is also provided (LSA-SAF PUM VEGA, 2008).

LSA-SAF products represent an interesting alternative to SPOT-VGT or MODIS for meso-scale applications because of its relatively high generation frequency, its near-real time availability and its improved time stability (LSA-SAF PUM VEGA, 2008). LSA-SAF LAI and FVC have been produced routinely since August 2005 with successive algorithm (VEGA) improvements related to methodology (VEGA v2.0, September 2006), input data quality (December 2006), and post-processing (VEGA v2.1, May 2008).

3 Methods

3.1 Exploitation of the LSA-SAF biophysical variables

LSA-SAF LAI and FVC are provided daily at the MSG/SEVIRI spatial scale over the whole field of view. At that scale, landscapes can be very heterogeneous, especially over Europe, and one pixel can represent a mixed signal of different ecosystems or PFTs. This information cannot be used as such in SVAT-type models because more details on each PFT is necessary to compute surface fluxes. In addition, there can be some gaps in the products or pixels in the images could be unprocessed, because the models require continuous, stable and consistent LAI time series. It is therefore needed to implement a procedure able to retrieve LAI at sub-pixel (or PFT level), and to cope with continuity and stability issues. A two-steps procedure is implemented

Table 1. List of PFTs defined in ECOCLIMAP-I and used in the land surface model.

Code	PFT
1	Bare Soil
2	Rocks
3	Snow (Permanent)
4	Deciduous Broad leaf Forest (DBF)
5	Evergreen Needle leaf Forest (ENF)
6	Evergreen Broad leaf Forest (EBF)
7	C3 crops
8	C4 crops
9	Irrigated crops
10	Grassland (G)
11	Swamp areas and bogs

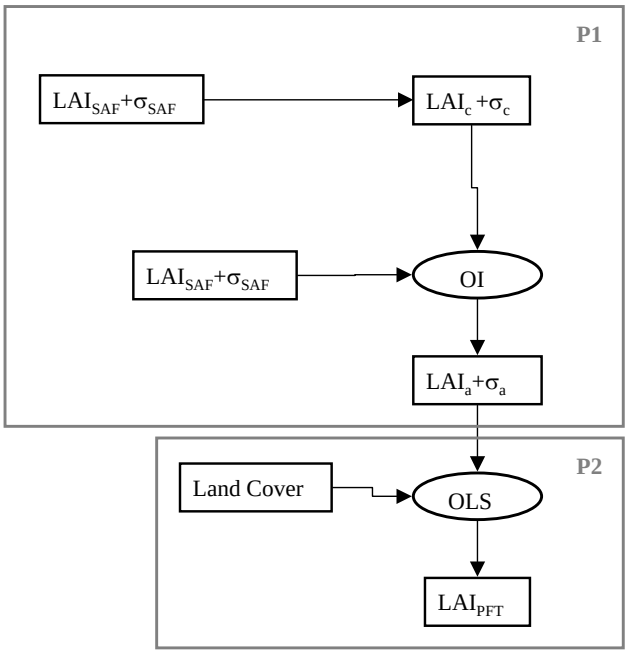

Fig. 1. Flowchart of the two-steps procedure to obtain LAI for each PFT in a given MSG/SEVIRI pixel. First, continuous and consistent LAI series are created at pixel level, LAI_a, using a 4-yr climatology from LSA-SAF LAI, LAI_{SAF}, actual LAI_{SAF}, and an optimal interpolation (OI) method. Then, the pixel LAI is decomposed into LAI_{PFT} for each PFT contributing to the pixel area, using a land cover map, LAI_a and an ordinary least square method (OLS).

to, first, provide LSA-SAF LAI maps consistent in time, and then, to compute vegetation parameters for each PFT of the considered pixel. A schematic view of the process is shown in Fig. 1.

For every pixel, it is necessary to build continuous and consistent LAI time series as close as possible to the actual LSA-SAF LAI product, LAI_{SAF}. First, an annual LAI climatology is built pixel-wise using daily LSA-SAF LAI images from 2007 to 2010. The climatological year is divided in periods of 10 days. For each 10 days period, a mean LAI, LAI_c, is calculated pixel-wise along with an error bar, σ_c, corresponding to the standard deviation of the LSA-SAF LAI sample used.

Even if snow cover is detected, some spurious data, occurring especially during the 2007–2008 winter in northern latitudes and over coniferous forests, still persist. Similar problems have been encountered by Jiang et al. (2010) with the NOAA satellite. In May 2008, LSA-SAF changed the algorithm to VEGA v2.1 to screen those data by applying a post-processing on the problematic areas. However, in order to take advantage of the longest time series available, the spurious data are filtered out using a threshold. Winter LAI higher than 85 % of the mean summer value are filtered out. The extent of the filtering period is based on the collection of the spurious data: it is longer for Northern European countries (e.g. Sweden, Finland) and shorter for the European mid-latitude countries (e.g. Germany, France).

In order to get continuous time series needed by operational models (Jiang et al., 2010), a linear interpolation is applied to both LAI values and standard deviations to fill the gaps in the climatological series.

Finally, for each actual LSA-SAF LAI, an optimal interpolation scheme (Gu et al., 2006) is applied. In our case, LSA-SAF LAI time series are more stable in time than the MODIS LAI (LSA-SAF PUM VEGA, 2008), and the LAI climatology is created from 4 yr of data. Appropriate weighting factors have been tuned and the error on the climatology, σ_c, is multiplied by 2.5 and noted $\tilde{\sigma}_c$. Consequently, the weight of the climatology is decreased to better follow the daily remote sensing product. The result is a LAI for each pixel (LAI_a); corrected using a background climatological information (Eq. 1). Therefore, most dubious data are removed, the time series are smooth and gaps are filled.

$$LAI_a = \frac{\tilde{\sigma}_c^2}{\sigma_{SAF}^2 + \tilde{\sigma}_c^2} \cdot LAI_{SAF} + \frac{\sigma_{SAF}^2}{\sigma_{SAF}^2 + \tilde{\sigma}_c^2} \cdot LAI_c. \quad (1)$$

As in Gu et al. (2006), when $|LAI_{SAF} - LAI_c| > 2\sqrt{\sigma_{SAF}^2 + \tilde{\sigma}_c^2}$, LAI_{SAF} is unusable and $LAI_a = LAI_c$.

An ordinary least-square algorithm (OLS) is then applied to derive LAI for each PFT, using LSA-SAF LAI and PFT percentages over a neighbourhod of 9 (3×3) or 25 (5×5) pixels (see Appendix A). Two assumptions are needed: (1) the percentage of each PFT in one pixel represents exactly the real cover of the land surface, (2) the vegetation parameters, e.g. LAI, in close neighbourhood are assumed to be homogeneous. This hypothesis is reasonable if we consider that, in a close neighbourhood, meteorological and climatic conditions are similar, and one can assume the growth of the natural vegetation will be the same for one specific plant type. For human-forced vegetation, like for crops, the assumption can still hold if we assume that agricultural practices are

homogeneous in the region of interest, which is often the case for large areas.

Repeating the operation by moving the size-defined neighbourhood by one pixel at a time, we obtain a smoothed spatial average estimate of LAI for each PFT.

Special attention has been paid to the correct handling of remote sensing derived vegetation products in the land surface model, avoiding a simultaneous variation of LAI and Fveg (Oleson and Bonan, 2000; van den Hurk et al., 2003; Jiang et al., 2010; Miller et al., 2006) and defining the LAI for the vegetation needed by the model from the remote sensing derived product (Ge, 2009). Fveg is therefore constant and is built pixel-wise using the complement to the absolute minimum LSA-SAF FVC over 2007 and 2008. Assuming that the bare soil fraction has a nul LAI, consistent handling of LAI for the land surface model is ensured through OLS.

Because of the uncertainty of land cover maps due to misclassification (e.g. Jung et al., 2006), some erroneous LAI could be estimated from the least-square algorithm. We propose to assess the impact of the uncertainty on the retrieved LAI_{PFT} at 120 pixels selected randomly over the *Euro* window. The uncertainty is evaluated by applying the LAI decomposition using 3 different land cover maps for 2007. ECOCLIMAP-I, MODIS (MCD12Q1) and GlobCover (Bicheron et al., 2006, 2008) land cover maps, available at 1000, 500 and 300 m resolution respectively are considered here. For each PFT in each selected pixel, the PFT percentage differences (rescaled to Fveg) are computed and the time correlation and root-mean square difference (RMS) between the LAI_{PFT} series obtained from the 3 land covers are estimated, by PFT and by pixel. Results are presented in Sect. 4.2.

Since a PFT is a *class* of vegetation (Alton, 2011; Williams et al., 2009), pixel-to-pixel variation of LAI_{PFT} may occur, and could affect the retrieval. In Sect. 4.2, we analyze those variations. For a given PFT, only the LAI value of homogeneous pixels (PFT covers more than 99 % of the pixel surface), LAI_{Hg}, are taken into account. A reference sample of LAI_{Hg} is selected randomly from the total population. The difference between the reference sample and the remaining LAI_{Hg} gives a probability density function of LAI_{PFT} variability as a function of the distance to the reference, up to 3 pixels, being the maximum size of the neighbourhood window used in OLS (3×3, 5×5 and 7×7). As the probability density functions are nearly symmetric and unimodal, very close to a gaussian, we study the normalized standard deviation as a proxy for the uncertainty. Results are given in Sect. 4.2.

3.2 Evapotranspiration modelling and validation strategy

The impact of using LSA-SAF LAI instead of ECOCLIMAP-I database in the land surface model is evaluated at two different scales: at local scale and over a larger region covering a sample of different vegetation dynamics and climate.

Table 2. In-situ eddy covariance observations used in this study.

Site	Country	Years	Reference
Skukuza	S. Africa	2008–2009	Kutsch et al. (2008)
Vielsalm	Belgium	2007–2008	Aubinet et al. (2001)
Tojal	Portugal	2007	Pereira et al. (2007)
Puéchabon	France	2007	Joffre et al. (1996)
Agoufou	Mali	2007	Merbold et al. (2009)
Tchizalamou	R. Congo	2007	Merbold et al. (2009)
Wetzstein	Germany	2007	Rebmann et al. (2010)
Sodankylä	Finland	2007	Suni et al. (2003)
Demokeya	Sudan	2007–2009	Sjöström et al. (2009)

Locally, the impact is quantified against measurements at different local observation sites equipped with eddy covariance devices. Results of point scale simulations are compared to in-situ observations of latent heat flux, LE (list of stations in Table 2), equivalent to ET. Four sites are situated in Africa and five in Europe, with a good sample of different climates. The four sites in Africa are installed in a savannah landscape, but with different precipitation regimes ranging from mostly dry (Agoufou) to mostly wet (Tchizalamou). The European sites are situated in mediterranean (Puéchabon and Tojal), temperate (Vielsalm and Wetzstein) and boreal (Sodankylä) regions. Four European stations monitor the exchanges between a forest stand and the atmosphere: coniferous forest (Wetzstein and Sodankylä), evergreen forest (Puéchabon) and mixed forest (Vielsalm). The station of Tojal monitors exchanges over a C3/C4 grassland site. Most of the sites selected have a large homogeneous fetch, that allows a good representativity of the measurements.

At the selected sites, the model is forced as described in Sect. 2.1. However, in order to better assess the impact of LAI on the simulations, in-situ measurements are used for radiation and precipitation input when available. ERA-Interim precipitation rates are used for Agoufou and Vielsalm sites. Precipitation is especially important in semi-arid environments (Merbold et al., 2009), and the more accurate the input is the better is the model output. Soil moisture and soil temperature for the four soil layers are initialized with ERA-Interim analysis, and the model is run over one year before the analyzed run. Model parameters are not tuned for the selected sites, and the general parameterization for a global simulation is set.

At large scale, we evaluate the impact on ET by comparing the daily ET rates over a latitudinal transect crossing a vegetation density gradient. As ECOCLIMAP-I gives an oversimplification of LAI spatial variability over Africa (Kaptué Tchuente et al., 2010); we compare the simulations along a north–south transect in West Africa, 15° N to 6° N, 0° E, for the year 2007 that samples a full range of vegetation dynamics from an evergreen humid forest to desert. This exercise

is especially relevant in the context of the growing interest in the land surface monitoring in Western Africa, where quantitative remote sensing is expected to play an important role (Stisen et al., 2008; Boone et al., 2009). The land surface model is forced as described in Sect. 2.1 and half-hourly simulated LE are converted to ET rates and daily cumulated.

As there is no ET observation dataset to validate/verify the improvements at large scale over West Africa, other remote sensing products are of interest for output verification. We can assess the impact of using LSA-SAF LAI in the land surface model by comparing other modeled variables to complementary remote sensing derived data. The modelled *skin* temperature from H-TESSEL can be compared to the land surface temperature derived from infra-red sensors. Even if the model *skin* temperature has not the exact same physical meaning as the radiative land surface temperature measured by the satellite (LST), it is often considered to be comparable (e.g. Ghent et al., 2011) and LST is used for indirect model's verification (e.g. Edwards, 2009; Jimenez et al., 2008). A particular interest of LST for ET verification is its link with soil moisture. For example, during observation campaigns in Western Africa, LST was linked to the soil moisture retrieved with passive microwave sensors (Kergoat et al., 2011). In addition, LST from MSG has been used to derive evaporative fraction (Stisen et al., 2008), which should likely be mainly driven by soil moisture in that region. LSA-SAF provides land surface temperature images (LSA-SAF LST) every 15 min, based on MSG/SEVIRI at the sensor resolution (Trigo et al., 2008). LST product is suitable for comparison as it is provided with the same spatial resolution.

To avoid the effect of short-term fluctuation of the temperature or cloud contamination, daily surface heating rates, expressed in $\mathrm{K\,h^{-1}}$, are calculated from LSA-SAF 15 min LST data, and from the simulated 30 min skin temperature separately. The heating rates are the slope of the linear fit through the land surface temperature data between sunrise and noon LT.

4 Results

4.1 Comparison of ECOCLIMAP-I and LSA-SAF LAI

To show the advantages of the new LSA-SAF products, we illustrate comparison of LAI with ECOCLIMAP-I database. The mean monthly LAI from ECOCLIMAP-I and LSA-SAF are compared by PFT (Fig. 2) in Europe for March to November 2007. Each monthly LAI is based on homogeneous pixels, i.e. pixels occupied by exclusively one PFT, and six LSA-SAF LAI images per month. In addition, the monthly spatial and temporal LAI variability is estimated from LSA-SAF LAI. In Fig. 2, it is shown that ECOCLIMAP-I LAI has a bias of about $1\,\mathrm{m^2\,m^{-2}}$ compared to LSA-SAF LAI. It is especially visible for evergreen coniferous forests during the summer months and crops for the beginning of autumn. This bias had also been reported in comparison with other products and in-situ data (Garrigues et al., 2008). A larger variability is found in LSA-SAF LAI for Swamp areas, forests and partly for grasslands. For crops, the variability is comparable.

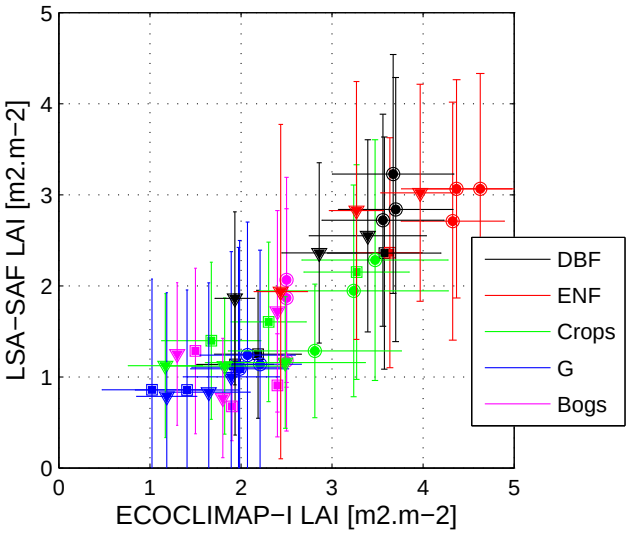

Fig. 2. Comparison of monthly mean and variability of LAI between ECOCLIMAP-I and LSA-SAF, for March to November 2007 over Europe. March to May (□), June to August (○), September to November (▽)

For Europe, small differences are observed in average, probably because the number of defined ecosystems in the land cover map is sufficiently high. However, over Africa, LSA-SAF LAI provides more spatial variability compared to the database. As an example, we compare the LAI variability of PFTs from 3 different homogeneous ECOCLIMAP-I ecosystems (tropical African grassland, semi-arid African grassland, and Nile Valley and desertic crops). Three LSA-SAF LAI images are selected for comparison on three different dates (15 April, 15 August and 15 December), and the LAI distribution is compared to the single value given by ECOCLIMAP-I monthly estimates (Fig. 3). For tropical African grassland, LAI given by ECOCLIMAP-I ranges between 2.0 and 3.0, while LSA-SAF LAI gives in one image a distribution ranging between 0 and 4. For the ecosystem Nile Valley and desertic crops, LSA-SAF LAI analysis shows a double peaked distribution poorly represented by the LAI database climatology. The difference is especially striking for April. The database gives a LAI of 0.5, while the peak reaches its maximum around 2.8. Those differences will inevitably impact on land surface model applications at MSG/SEVIRI scale.

LSA-SAF LAI product allows a better temporal representation of the inter-annual LAI evolution. As an example, we compare the LAI time series from ECOCLIMAP-I and LSA-SAF over a pixel in Western Africa corresponding to the

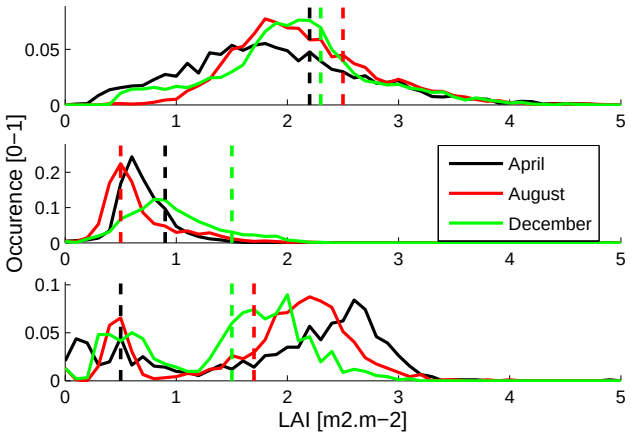

Fig. 3. Distribution of LSA-SAF LAI (continuous lines) against ECOCLIMAP-I monthly values (dashed vertical lines) for 3 dates (15 April, 15 August and 15 December 2007) for 3 homogeneous ecosystems: tropical African Grassland (top), Semi-Arid African grassland (middle) and Nile Valley and desertic crops (bottom).

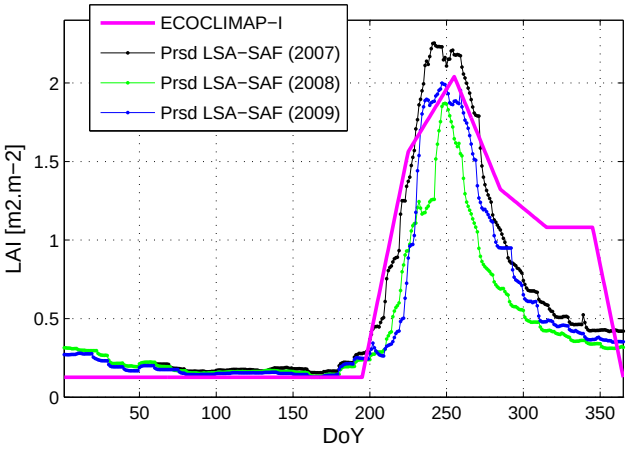

Fig. 4. Time series comparison of processed LSA-SAF LAI (Prsd LSA-SAF) for 2007, 2008 and 2009, and re-scaled and linearly interpolated ECOCLIMAP-I LAI for a pixel in Western Africa (15.29° N, 1.49° W).

ground measurement station Agoufou (15.29° N, 1.49° W) for 2007, 2008 and 2009. The variability is mostly driven by the occurence of rain during the wet season. In the comparison LSA-SAF LAI has been rescaled by the complement to unity of the minimum fraction of vegetation, while ECOCLIMAP-I LAI has been rescaled to the range of LSA-SAF LAI, and linearly interpolated. In Fig. 4, we observe the time shifts in the wet season onset, as well as the differences in duration of that season and LAI peak. Differences up to 10 days in the shift are observed for the wet season onset (Day 200–210). During the onset of the dry season (DoY 260–270), there is a large difference between ECOCLIMAP-I LAI and LSA-SAF LAI, with a sharp decrease of LSA-SAF LAI. Impact on the ET simulation with the land surface model is assessed in Sect. 4.3.

4.2 Retrieval of sub-pixel leaf area index

As presented in Sect. 3, LSA-SAF LAI needs to be processed to obtain continuous and coherent time series. We illustrate that process on one specific LAI time series over Wetzstein, a forested site in Europe (Fig. 5). The MSG/SEVIRI pixel is mainly composed of coniferous forest. LSA-SAF LAI (red points) presents unrealistic high values in the 2007–2008 winter. During the next winters, most of those unrealistic estimates have been screened out in the product. The LAI climatology (black points) follows the trend given by LSA-SAF LAI, with very high values in winter. Using the filter, we remove all the spurious data, and a linear interpolation is applied. After correction, the optimal interpolation procedure is applied to produce the LAI analysed, LAI_a.

With the new pixel estimates LAI_a, the method to decompose at sub-pixel scale is applied. However, as mentionned, the method is subject to two sources of error. The impact of the uncertainty of the land cover map and of the pixel-to-pixel LAI variability of PFTs is assessed here.

The impact of the land cover map uncertainty on the LAI retrieval is represented in Fig. 6, where the relation between the mean PFT percentage obtained from the three land cover maps and the RMS of the LAI time series for the 120 pixels defined in Sect. 3.1 is shown. The mean correlation decreases with a smaller PFT percentage, and RMS increases. It implies that land cover differences have little impact on the retrieved LAI for the dominant PFTs, but that it has a big impact on the less dominant PFTs. In addition, we observe less uncertainty for crops class than for evergreen forests compared to the mean.

As shown in Fig. 7, effect of enlarging the neighbourhood to 5×5 and 7×7 pixels for OLS lessens the impact of land cover uncertainty: the correlation decreases only to 0.5 for very small PFT percentages. The effect of enlarging to 7×7 has no big impact compared to 5×5.

The impact of the pixel-to-pixel LAI variability by PFT is represented in Fig. 8. For each homogeneous PFT represented in Europe and Africa, the normalized standard deviation increases with the OLS neighbourhood size (Fig. 8). For Europe, the variability inside a 3×3 neighbourhood ranges between 13 % and 19 %. Increasing the pixel number to 5×5 degrades the quality of the assumption for all PFTs. The variability increases gradually from 3×3 to 7×7 for C3 crops and grasslands. For Africa, the uncertainty is much less than for Europe, ranging between 5 % and 9 % for all classes in the case of the 3×3 neighbourhood. In addition, enlarging the neighbourhood to 5×5 or 7×7 has no big impact for most PFTs in Africa, except for grassland in Northern Africa. Variability could not be assessed for deciduous broadleaved forests over Africa because no african ecosystem defined in ECOCLIMAP-I is homogeneously covered by that PFT.

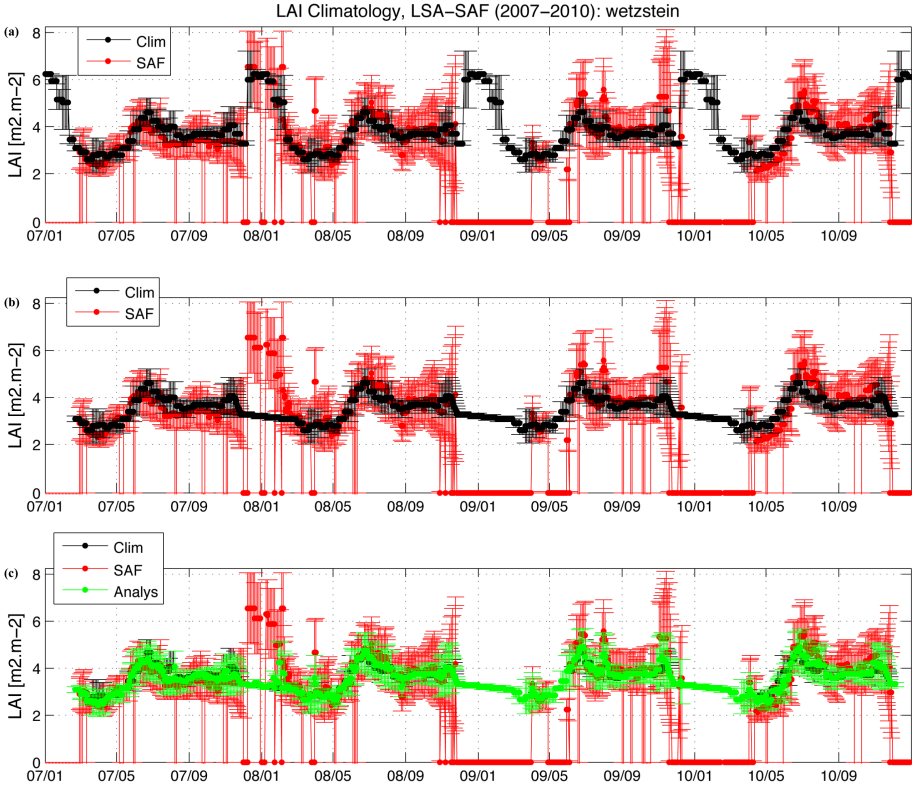

Fig. 5. Illustration of the pre-processing of LSA-SAF LAI images on a test case over a forest (Wetzstein) in Germany. **(a)** A 10-days composite (black) is derived from LSA-SAF LAI daily data (red). **(b)** Spurious data are filtered out, and linear interpolation is applied to create the climatology, LAI_c (black). **(c)** At last, an optimal interpolation scheme (OI) is applied using the climatology and the actual LSA-SAF LAI, LAI_{SAF}, to provide the analysed LAI, LAI_a.

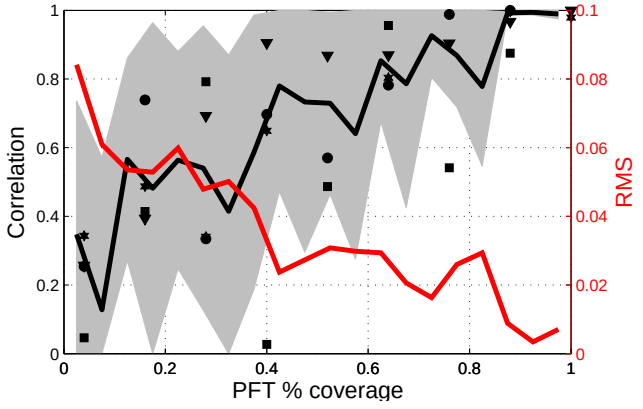

Fig. 6. Mean correlation (black line) between LAI time series obtained using ECOCLIMAP-I, GLOBCOVER and MODIS land covers, and its dependence in the PFT percentage in a given MSG/SEVIRI pixel for a 3×3 neighbourhood. The grey shaded area represents the dispersion of the correlation. PFT dependent correlation is superimposed (DBF: $\circ$, ENF: $\square$, crops: $\triangledown$, grass: $*$). In addition, RMS resulting from the comparison of the time series is shown in red.

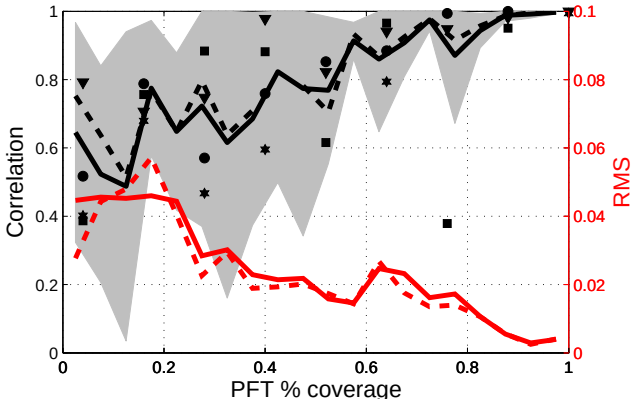

Fig. 7. Same as Fig. 6, but for a 5×5 (solid) and 7×7 (dashed) neighbourhood.

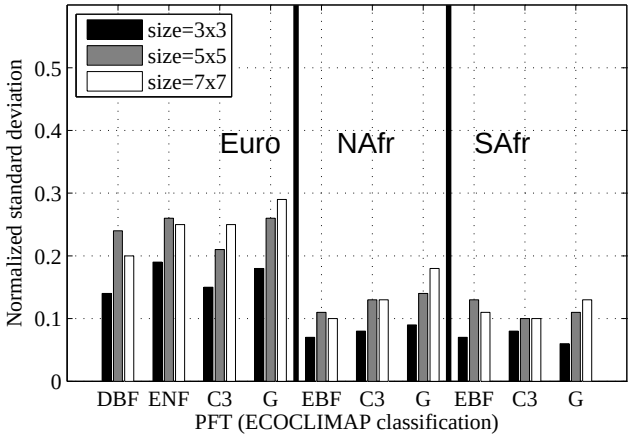

Fig. 8. Normalized PFT intra-variability (standard deviation) of LAI in function of the neighbourhood size for Europe (Euro) and Africa (NAfr and SAfr).

The method proposed in Sect. 3 leads to a more robust estimate of LAI_{PFT} when applied over a larger neighbourhood (Fig. 7), since impact of land cover map uncertainty is reduced. However, at least for Europe, LAI variability of a given PFT increases with the size of the neighbourhood (Fig. 8). Therefore, depending on the application, a compromise has to be found between accuracy and robustness. In applications involving spatial resolution equal to MSG/SEVIRI, the smallest size is obviously preferred since it implies less uncertainty. However, it has been shown that the quality of the OLS algorithm is decreasing along with PFT occupation fraction, due to the land cover uncertainty. Therefore, in waiting for a better agreement between land cover maps, a correction has to be applied, to estimate a reliable LAI_{PFT} even for the least contributing PFT to the total pixel ET. A corrected estimate, $LAI_{PFT,PostP}$, is derived from a weighted average of LAI_{PFT} and a reference estimate, LAI_R (Eq. 2). The weight α (Eq. 3) is proportional to the PFT percentage, and we choose it to be the linear regression of Fig. 6.

$$LAI_{PFT,PostP} = \alpha \cdot LAI_{PFT} + (1-\alpha) \cdot LAI_R \quad (2)$$

$$\alpha = \min(0.75 \cdot PFT_{\%} + 0.32, 1) \quad (3)$$

LAI_R could be the LAI pixel value, LAI_a, or the LAI value corresponding to the nearest pixel homogeneous of that PFT, LAI_{Hg}. Since African ecosystems are mostly a mix of PFTs, LAI_a is adopted. For Europe, clear homogeneous PFTs can most of the time be identified and isolated, and LAI_{Hg} is preferred. This choice is further discussed in Sect. 5.

4.3 Impact on modelled evapotranspiration

Statistical results for the 30 min model estimates of LE are presented in Table 3. Statistical scores show an improvement in the modelling of the surface latent heat flux, or equivalently ET, especially for semi-arid regions where the signal shows an interannual variability in amplitude and phase. The largest improvements are observed for Skukuza and Agoufou sites, with a significant decrease of the global bias compared to data (-37 to $-6\,W\,m^{-2}$ for Skukuza, and -32 to $-18\,W\,m^{-2}$ for Agoufou) as well as an improved Nash-Sutcliffe (NS) index (0.46 to 0.60, and 0.26 to 0.45, respectively) (Nash and Suttcliffe, 1970). Even if the scores are largely improved in the Agoufou comparison, most of the remaining bias is due to non ideal precipitation forcing, i.e. ERA-Interim in that simulation. The other simulations over African sites, i.e. Demokeya and Tchizalamou, also show an improvement of the statistical scores when compared to data (NS: 0.53 to 0.62, and 0.51 to 0.53, respectively). Those results confirm the findings of Kahan et al. (2006) over the Sahel region in Western Africa.

Table 3. Comparison of simulations with ECOCLIMAP-I (ECO) or LSA-SAF LAI (LSA) against 30 min observed LE ($W\,m^{-2}$): statistical scores: correlation coefficient (ρ), root mean square error (RMSE), bias and NS (Nash and Suttcliffe, 1970). Improved NS with LSA compared to ECO are in bold.

Station	Mode	ρ	RMSE	Bias	NS
Skukuza	ECO	0.754	85.07	−37.86	0.46
	LSA	0.787	73.25	−6.25	**0.60**
Demokeya	ECO	0.768	53.41	−18.55	0.53
	LSA	0.795	48.39	−5.26	**0.62**
Tchizalamou	ECO	0.760	60.14	3.16	0.51
	LSA	0.775	58.68	9.11	**0.53**
Agoufou	ECO	0.612	83.56	−32.40	0.26
	LSA	0.695	72.42	−18.37	**0.45**
Puéchabon	ECO	0.817	44.42	−9.29	0.61
	LSA	0.85	40.83	2.71	**0.67**
Tojal	ECO	0.849	41.98	−5.94	0.66
	LSA	0.828	45.37	−6.95	0.61
Vielsalm	ECO	0.747	46.89	10.88	0.47
	LSA	0.712	47.75	8.73	0.46
Wetzstein	ECO	0.832	53.14	−26.78	0.57
	LSA	0.850	48.83	−22.94	**0.64**
Sodankyla	ECO	0.711	29.59	−8.68	0.39
	LSA	0.735	28.16	−11.08	**0.44**

As an example, we present in Fig. 9, the time series of the simulated and observed LE in Demokeya for the year 2007 to 2009. The simulation is clearly improved with the use of LSA-SAF LAI, with a better match during the wet season. Also, the simulations of LE during the dry season is closer to the observations.

Results over Europe show an improvement for 3 sites over the 5. In Puéchabon, the scores are well improved, with a global bias reduction, from -9 to $3\,W\,m^{-2}$, and a better NS, from 0.61 to 0.67. As well, the results are improved

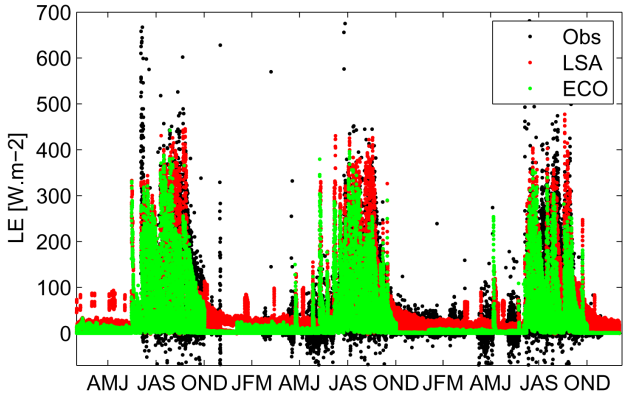

Fig. 9. Comparison of LE for Demokeya for 2007, 2008 and 2009; observed in (Obs: black), simulation using ECOCLIMAP-I (ECO: green), simulation using LSA-SAF LAI (LSA: red).

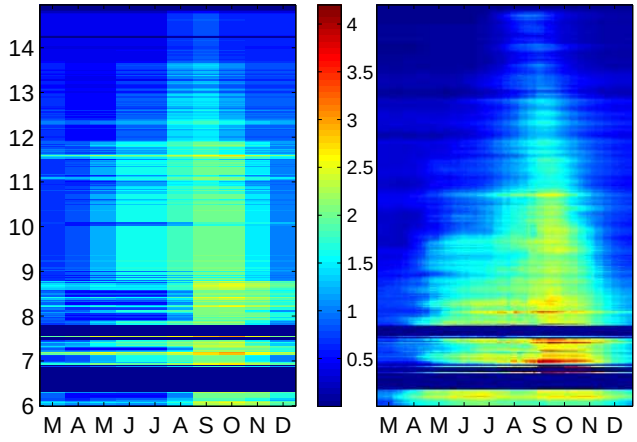

Fig. 10. LAI evolution (March to December 2007) along the north–south transect in West Africa from 15° N to 6° N: ECOCLIMAP-I (left) and LSA-SAF LAI (right)

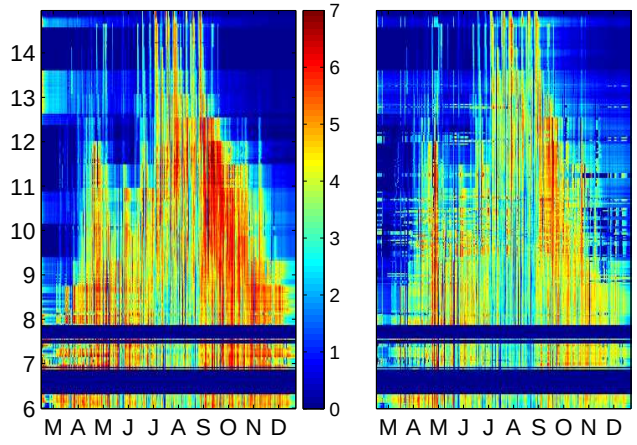

Fig. 11. Simulations along the north–south transect in West Africa from 15° N to 6° N: daily ET [mm] simulated using ECOCLIMAP-I (left) and LSA-SAF LAI (right).

for 2 forested sites in different climates, i.e. Wetzstein and Sodankylä. For Tojal and Vielsalm, the model performs well with ECOCLIMAP-I and the statistics are either slightly degraded or equal.

The evolution of the LAI on the latitude gradient is shown in Fig. 10 for monthly ECOCLIMAP-I and daily LSA-SAF. The northern bound of the transect is completely arid with no vegetation. Southwards, vegetation is seasonal, with longer periods of vegetation cover, and higher amplitudes. The global pattern for ECOCLIMAP-I and LSA-SAF is similar, however, the most striking difference is seen on the length of the vegetation period that is noticeably shorter for LSA-SAF at highest latitudes. Between 6° N and 8° N, the transect meets lakes, resulting in zero LAI as observed from the dark blue stripes in the figures.

The evolution for 2007 along the transect is shown in Fig. 11, when using ECOCLIMAP-I and LSA-SAF LAI, respectively. The global pattern is mostly the same, as ET is driven by precipitation. However, large differences are found between September and December (also in April), with higher ET produced using ECOCLIMAP-I database.

An indirect evaluation of the changes is based on the comparison of the daily surface heating rates modelled and derived from the satellite. The heating rates are shown in Fig. 12. Vegetated areas are characterized by lower mean surface heating rates than bare soil. As well, surface heating rates are said to be increased with decreasing soil moisture (Stisen et al., 2008). The global pattern with the contrast low/high heating rate is seen in the three images. Good correspondence is found in the patterns of both simulations. That is probably due to the same precipitation forcing for the model. The absolute differences between simulated heating rates and those derived from LSA-SAF LST are represented in Fig. 13. A closer agreement, especially with a global lower bias, is found with the skin temperature simulated using LSA-SAF LAI than with ECOCLIMAP-I when compared to LSA-SAF derived heating rates, suggesting than simulation is improved using LSA-SAF LAI.

5 Discussion

Different aspects of the method to use LSA-SAF biophysical variables in H-TESSEL and its application for ET monitoring are discussed, especially in the perspective of continuous operational monitoring.

5.1 Retrieval stability of the biophysical variables

With one observation every 15 min over the same location, a higher level of stability of biophysical variables is reached when derived from MSG/SEVIRI comparatively to polar orbiters. Indeed, it has been shown that LSA-SAF LAI was more reliable than SPOT-VGT over central Africa where cloud cover is most frequent (Pekel et al., 2010). However, stability problems, that have been addressed by the methodology proposed in Sect. 3, are found in the original LSA-SAF

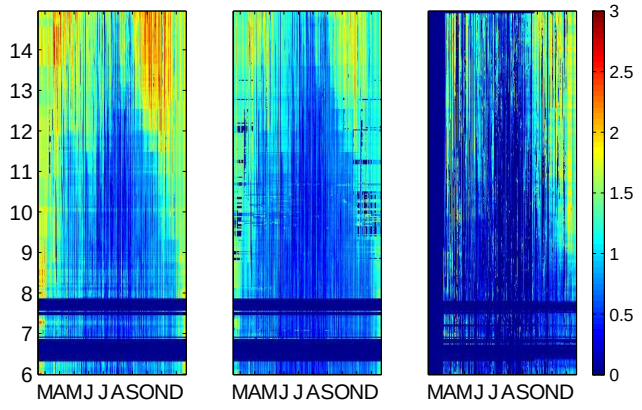

Fig. 12. Daily morning surface heating rates [K h^{-1}] for a transect in West Africa from 15° N to 6° N: simulation using ECOCLIMAP-I (left) or LSA-SAF LAI (middle), obtained from LSA-SAF LST (right).

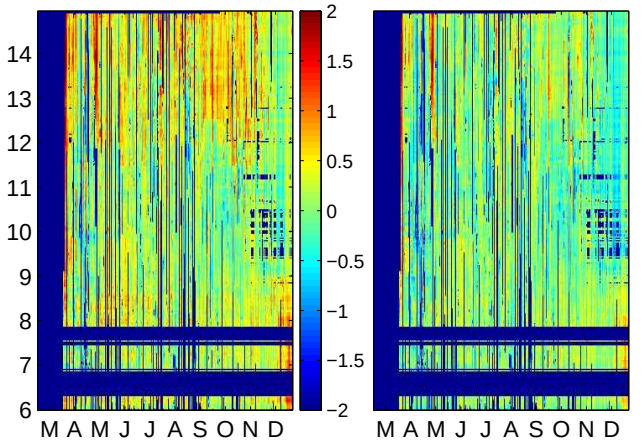

Fig. 13. Differences in the daily morning surface heating rates [K h^{-1}] (same transect Fig. 12): simulated heating rates using ECOCLIMAP-I vs. LSA-SAF LST (left), simulated heating rates using LSA-SAF LAI vs. LSA-SAF LST (right).

time series for Northern European regions covered by coniferous forests for 2007 and 2008, while further production by LSA-SAF made used of a filter to screen out those spurious data. Similar problems are encountered for the generation of other biophysical products. GLOBCARBON LAI products show unexpected variations for boreal forests, with possible overestimated LAI (Garrigues et al., 2008). The MODIS Collection 4 and 5 LAI products present a spurious seasonal variability over boreal forests due to the low data availability with weak illumination, extreme solar zenith angles conditions, snow and cloud contamination (Yang et al., 2006a,b; Tian et al., 2006; Garrigues et al., 2008) and low spatial continuity due to regular failures from the main retrieval algorithm (Garrigues et al., 2008). Retrieval problems are also encountered during peak seasons over deciduous broadleaf forests (Garrigues et al., 2008). Corrections and smoothings are therefore needed for an optimal use in land surface models (Gu et al., 2006).

5.2 Towards an operational use of LSA-SAF biophysical products

In Sect. 4.2, it has been shown that the land cover map uncertainty has an effect on the LAI retrieval at sub-pixel scale, and that a correction need to be applied to obtain reliable estimates using a reference. It has been proposed, for Europe, to use as reference the LAI of the nearest homogeneous pixel, LAI_{Hg}. However, the success of it depends on the relative invariability of LAI for one PFT in a neighbourhood, and therefore on finding a LAI_{Hg} within a close area. The analysis of (1) its variability within an increasing area (Fig. 14) and (2) the distribution of distance to the nearest LAI_{Hg} (Fig. 15) leads to PFT specific conclusions in using it as a correction for the retrieved LAI_{PFT}. As expected, the relative variability increases with distance for every PFT, with the sharpest difference within the first five pixels. In addition, the total increase is most important for grasslands (up to 55 % variability 30 pixels away) and crops (45 %), while it is less for forests (32 % and 37 %).

Figure 15 represents the distribution, based on ECOCLIMAP-I land cover map, of the distance from each pixel to the closest homogeneous pixel for the same PFTs in Europe. For every PFT, the number of occurence decreases with the distance. The decrease is sharp for crops, with more than 70 % of homogeneous pixels no further than six distance units. For the other types, there are less homogeneous pixels and the decrease is quasi linear. In 90 % of the cases, the nearest homogeneous pixel is found at a distance of 16 pixels (Crops), 30 (ENF), 31 (G), and 33 (DBF).

From Figs. 14 and 15, we conclude that (1) the farther the homogeneous pixel used for correcting the OLS solution comes from, the larger is the introduced error, especially for crops and grasslands; (2) the most uncertain correction in the post-processing will be for grasslands in Europe. LAI_a is used as reference in that case, as well as for PFTs not represented by an homogeneous pixel in the neighbourhood.

We therefore propose a post-processing scheme, summarized by a flowchart in Fig. 16, integrating the results discussed here. If the area to process is Europe, C3 crops, and forests (DBF and ENF), LAIs are corrected with LAI_{Hg} (option 2). For grassland, if the distance is higher than 10 pixels, the pixel LAI is used as surrogate (option 1). For other PFT classes, i.e. C4 crops, irrigated crops and swamp areas, and for other areas, correction follows option 1.

5.3 A decreased uncertainty associated to LAI

While a thorough analysis of the uncertainty is out of the scope of the present paper, we compare estimates of LAI uncertainty for ECOCLIMAP-I ($\sigma_{LAI_{ECO}}$), and retrieved from

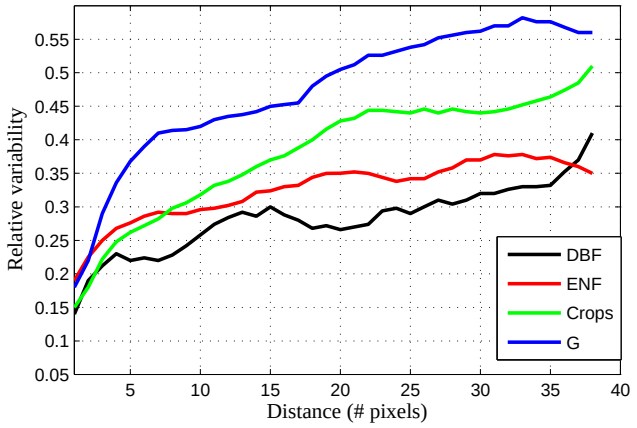

Fig. 14. Relative variability of LAI with distance (# pixels) to nearest homogeneous pixel, by PFT, i.e. C3 crops (black), DBF (red), ENF (blue), G (green), in Europe. A sliding average window of 5 distance units has been applied to the curve.

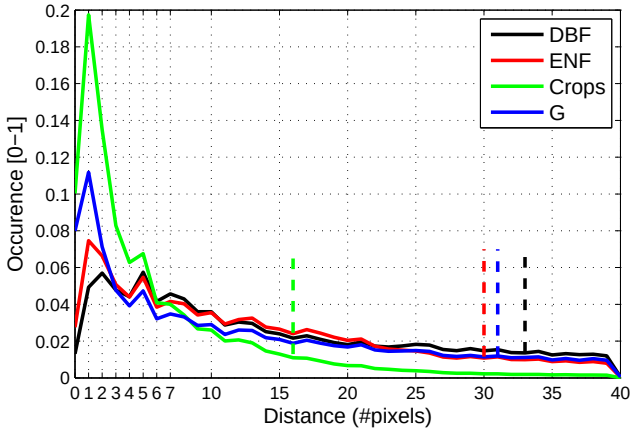

Fig. 15. Distance (# pixels) to nearest homogeneous pixel by PFT, i.e. C3 crops (black), DBF (red), ENF (blue), G (green), in Europe. Vertical dashed lines denote the 90 % of the cumulative distribution for each PFT (based on ECOCLIMAP-I).

LSA-SAF ($\sigma_{\mathrm{LAI_{SAF}}}$). $\sigma_{\mathrm{LAI_{ECO}}}$ can be evaluated with the spatial and temporal variability of LSA-SAF LAI. $\sigma_{\mathrm{LAI_{SAF}}}$ is the combination of the error on OLS, σ_{OLS}, and the error on assumptions, σ_{dist} (Fig. 8).

For Europe, LAI variability for a given PFT increases with the distance from a reference pixel (previous section). But, while for forests the variability remains almost steady with the distance, crops and grasslands are the most affected PFTs, giving a clear methodological advantage in using LSA-SAF LAI and a lower uncertainty. However, since ECOCLIMAP-I proposes a very fine classification into 92 ecosystems, e.g. 27 different types of crops and 21 types of grasslands, the difference between $\sigma_{\mathrm{LAI_{SAF}}}$ and $\sigma_{\mathrm{LAI_{ECO}}}$ is not expected to be large.

For Africa, Fig. 3 shows examples representative of wide areas in the *NAfr* region for a given year (2007).

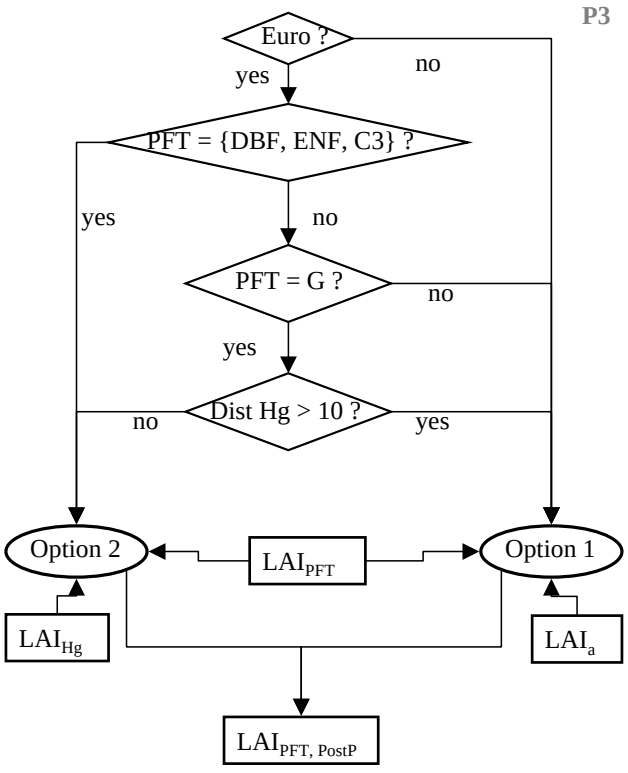

Fig. 16. Flowchart with post-processing steps of PFT derived LSA-SAF LAI, $\mathrm{LAI_{PFT}}$, to obtain a consistent LAI, $\mathrm{LAI_{PFT,PostP}}$. Option 1 refer to the correction of the retrieved LAI with the pixel estimate, while option 2 points to the nearest homogeneous pixel as the reference LAI.

Consequently, the deduced $\sigma_{\mathrm{LAI_{ECO}}}$ can be very large. Contrarily, $\sigma_{\mathrm{LAI_{SAF}}}$ is expected to be much less, because σ_{dist} is less than 10 %, and σ_{OLS} is very small due to the relative homogeneity of the landscape over the OLS neighbourhood. In particular, $\sigma_{\mathrm{LAI_{SAF}}}$ is expected to be much smaller than $\sigma_{\mathrm{LAI_{ECO}}}$ in semi-arid to arid environments in Africa, giving a more reliable LAI estimate for Sahel. That difference should obviously be exacerbated if we take into account the inter-annual variability not represented in ECOCLIMAP-I, as in Fig. 4.

5.4 Towards a continuous ET monitoring

The scheme presented in this paper and assessed with the land surface model has been developed to comply with requirements for near-real time applications. Applied to LSA-SAF LAI and FVC, it is convenient for ET monitoring through land surface modelling at spatial scales equal or coarser than MSG/SEVIRI. However, for a correct evaluation of LAI at PFT level, it is necessary to use a land cover map that proposes a sufficient accuracy in locating, classifying and decomposing into PFTs accepted by the land surface models. The gain in spatial resolution (ECOCLIMAP-I: 1 km; GlobCover: 300 m) and satellite overpass frequency

are clear advantages to obtain more accurate LAI at PFT level, reducing σ_{OLS}, and therefore providing an optimal input for land surface models.

In line with the monitoring concept, it would be necessary to have a clear assessment of the land cover changes, as it can affect our method. Regular updates of land cover would therefore be appreciated, to address land conversion issues like deforestation or fires.

6 Conclusions

In the present contribution, we show the benefits of using the daily biophysical variables derived from SEVIRI sensor aboard the geostationary satellite MSG for the evapotranspiration modelling and monitoring using the model H-TESSEL over Europe and Africa, compared to the use of the semi-static database ECOCLIMAP-I.

LAI maps from LSA-SAF and ECOCLIMAP-I are compared at different time and spatial scales, showing that ECOCLIMAP-I LAI presents less variability than LSA-SAF LAI, with respect to spatial coverage and temporal frequency. A rough analysis of the uncertainty on ECOCLIMAP-I LAI and LSA-SAF LAI over Africa suggests that LSA-SAF LAI is beneficial for land surface models intended for short time scales, e.g. half-hourly and daily, at MSG/SEVIRI resolution.

We propose a practical methodology to use the biophysical products LSA-SAF LAI and FVC in land surface models, correcting spurious data, filling gaps, and deriving sub-pixel LAI estimates needed by the models using a land cover map. Effects of the spatial scale and land cover map uncertainty on the method have been investigated, and results show that land cover uncertainty has an increasing impact on the less represented PFTs. The proposed method is shown to be more robust as the spatial scale considered is coarser. While waiting for land cover maps with reduced uncertainty, corrections of the errors on LAI by PFT are proposed for monitoring at the finest possible scale.

Given the respective features of both LAI sources investigated here, we have assessed the impact of using LSA-SAF LAI instead of ECOCLIMAP-I in H-TESSEL evapotranspiration simulations at MSG/SEVIRI resolution, both at local scale and at large scale.

Statistical scores of the comparison of simulated latent heat flux against local observations from ground measurement sites are improved in most cases, and especially in semi-arid climates. Amplitudes of anual cycles, as well as phase shifts are more correctly taken into account in the model compared to the use of the ECOCLIMAP-I database.

A 9-months simulation over a north–south transect in Western Africa using LSA-SAF radiation products and ERA-Interim meteorological variables, illustrates the impact of using LSA-SAF vegetation parameters compared to ECOCLIMAP-I database. An evaluation of the improvement is based on the similarity of the simulated skin temperature daily heating rates and the observed land surface temperature heating rates from MSG/SEVIRI, showing a better global agreement by using LSA-SAF biophysical variables.

Use of LSA-SAF LAI and FVC is therefore recommended for near-real time applications of land surface models working at the MSG/SEVIRI scale or coarser and intending at closely monitoring evapotranspiration. Moreover, it will improve the land surface model applications over Africa, capturing the full spatial, seasonal and inter-annual variability.

Appendix A

Least Square Algorithm application

Let $\mathbf{M}$ be the linear model matrix, representing the proportion $f_{i,j}$ for each pixel i of determined PFT j.

$$\mathbf{M} = \begin{pmatrix} f_{1,1} & \cdots & f_{1,N} \\ \vdots & \ddots & \vdots \\ f_{M,1} & \cdots & f_{M,N} \end{pmatrix} \tag{A1}$$

$\boldsymbol{Y}$ is the observation vector, which contains the LSASAF LAI_i estimates for the $\mathbf{M}$ considered pixels.

$$\boldsymbol{Y} = \begin{pmatrix} \mathrm{LSA-SAFLAI}_1 \\ \vdots \\ \mathrm{LSA-SAFLAI}_M \end{pmatrix} \tag{A2}$$

Now, let $\boldsymbol{X}$ be the solution vector containing the averaged values V_i over the domain for each involved ecosystem.

$$\boldsymbol{X} = \begin{pmatrix} V_1 \\ \vdots \\ V_N \end{pmatrix} \tag{A3}$$

Therefore, the problem has the following simple linear form (Eq. A4).

$$\mathbf{M} \cdot \boldsymbol{X} = \boldsymbol{Y} \tag{A4}$$

Taking into account the retrieval uncertainty of the LSA-SAF LAI and assuming it corresponds to the standard deviation of a normal error distribution, we scale the matrix $\mathbf{M}$ and the observation vector $\boldsymbol{Y}$ by weighting factors, $\sigma^{-1}_{\mathrm{SAF},i}$. A matrix $\mathbf{W}$ containing the weights is formed (Eq. A5), and new matrix $\mathbf{M}_w$ (Eq. A6) and vectors $\boldsymbol{Y}_w$ (Eq. A7) are defined. We get to solve Eq A8.

$$\mathbf{W} = \begin{pmatrix} 1/\sigma_{\mathrm{SAF},1} & 0 & \cdots & 0 \\ 0 & \ddots & \ddots & \vdots \\ \vdots & \ddots & \ddots & 0 \\ 0 & \cdots & 0 & 1/\sigma_{\mathrm{SAF},M} \end{pmatrix} \tag{A5}$$

$$\mathbf{M}_w = \mathbf{W} \cdot \mathbf{M} \tag{A6}$$

$$\boldsymbol{Y}_w = \mathbf{W} \cdot \boldsymbol{Y} \tag{A7}$$

$$\mathbf{M}_w \cdot \boldsymbol{X} = \boldsymbol{Y}_w \tag{A8}$$

Solving the linear set of equation using a least square method, we obtain the LAI for each PFT. The solution in the least square sense using the L2-norm, $\boldsymbol{X}$, is given by Eq. A9, whereby $\mathbf{M}_w^T$ is the transpose of $\mathbf{M}_w$.

$$\boldsymbol{X} = (\mathbf{M}_w^T \cdot \mathbf{M}_w)^{-1} \cdot \mathbf{M}_w^T \cdot \boldsymbol{Y}_w \tag{A9}$$

To fasten the numerical computation of the solution, as well as to avoid frequent difficulties in inverting large sparse matrices, we reduce the matrix $\mathbf{M}_w$ to its irreducible dimensions, corresponding to the number of pixels times the number of PFTs occupying the size-defined neighbourhood. If the matrix is non-invertible a singular value decomposition algorithm is applied.

Acknowledgements. The authors thank the Editor and the anonymous referees for their fruitful comments that have allowed to improve the readability of the manuscript. They are grateful to F. J. Garcia-Haro, F. Camacho de Coca and the LSA-SAF operating team to provide the LSA-SAF LAI and FVC images in near-real time, as well as DSSF, DSLF and AL. We also thank G. Balsamo for providing the H-TESSEL code, the in-situ data providers who could provide us with the necessary material for benchmarking, and ESA Globcover Project led by MEDIAS France for providing the Globcover land cover. The MODIS MCD12Q1 data were obtained through the online Data Pool at the NASA Land Processes Distributed Active Archive Center (LP DAAC), USGS/Earth Resources Observation and Science (EROS) Center, Sioux Falls, South Dakota (http://lpdaac.usgs.gov/get_data). This study has been done in the framework of the LSA-SAF project, funded at RMI by EUMETSAT and by ESA (contract e15066) under the PRODEX programme supported by the Belgian Sciences Policy, and in the framework of PROBA-VET project, supported by the Belgian Science Policy through the PROBA-V preparatory programme (contract CB/34/18).

Edited by: A. Loew

References

ALADIN International Team, The ALADIN project: Mesoscale modelling seen as a basic tool for weather forecasting and atmospheric research, WMO Bull., 46, 317–324, 1997.

Albergel, C., Calvet, J.-C., Mahfouf, J.-F., Rüdiger, C., Barbu, A. L., Lafont, S., Roujean, J.-L., Walker, J. P., Crapeau, M., and Wigneron, J.-P.: Monitoring of water and carbon fluxes using a land data assimilation system: a case study for southwestern France, Hydrol. Earth Syst. Sci., 14, 1109–1124, doi:10.5194/hess-14-1109-2010, 2010.

Alton, P. B.: How useful are plant functional types in global simulations of the carbon, water, and energy cycles?, J. Geophys. Res., 116, G01030, doi:10.1029/2010JG001430, 2011.

Aubinet, M., Chermanne, B., Vandenhaute, M., Longdoz, B., Yernaux, M., and Leitat, E.: Long term carbon dioxide exchange above a mixed forest in the Belgian Ardennes, Agr. Forest Meteorol., 108, 293–315, 2001.

Balsamo, G., Viterbo, P., Beijaars, A., van den Hurk, B., Hirschi, M., Betts, A. K., and Scipal, K.: A revised hydrology for the ECMWF model: Verification from field site to terrestrial water storage and impact in the integrated forecast system, J. Hydrometeorol., 10, 623–643, 2009.

Beljaars, A. C. M. and Viterbo, P.: The sensitivity of winter evaporation to the formulation of aerodynamic resistance in the ECMWF model, Bound.-Lay. Meteorol., 71, 135–149, 1994.

Bicheron, P., Leroy, M., Brockmann, C., Krämer, U., Miras, B., Huc, M., Nino, F., Defourny, P., Vancutsem, C., Arino, O., Ranéra, F., Petit, D., Amberg, V., Berthelot, B., Gross, D.: GLOBCOVER : a 300 m global land cover product for 2005 using ENVISAT/MERIS time series, Proceedings of the Recent Advances in Quantitative Remote Sensing Symposium, Valencia, September 2006.

Bicheron, P., Huc, M., Henry, C., Bontemps, S., and GLOBCOVER partners: GLOBCOVER: Products Description Manual, GLOBCOVER-PDM-I2.2, 2008.

Blyth, E., Best, M., Cox, P., Essery, R., Boucher, O., Harding, R., Prentice, C., Vidale, P. L., and Woodward, I.: JULES: a new community land surface model, Global Change NewsLetter, 66, 9–11, 2006.

Bonan, G. B., Levis, S., Kergoat, L., and Oleson, K. W.: Landscapes as patches of plant functional types: An integrated concept for climate and ecosystem models, Global Biogeochem. Cy., 16, 1021, doi:10.1029/2000GB001360, 2002.

Boone, A., de Rosnay, P., Balsamo, G., Beljaars, A., Chopin, F., Decharme, B., Delire, C., Ducharme, A., Gascoin, S., Grippa, M., Guichard, F., Gusev, Y., Harris, P., Jarlan, L., Kergoat, L., Mougin, E., Nasonova, O., Norgaard, A., Orgeval, T., Ottlé, C., Poccard-Leclercq, I., Polcher, J., Sandholt, I., Saux-Picart, S., Taylor, C., and Xue, Y.: The AMMA Land Surface Model Intercomparison Project (ALMIP), B. Am. Meteorol. Soc., 90, 1865–1880, 2009.

Brut, A., Rüdiger, C., Lafont, S., Roujean, J.-L., Calvet, J.-C., Jarlan, L., Gibelin, A.-L., Albergel, C., Le Moigne, P., Soussana, J.-F., Klumpp, K., Guyon, D., Wigneron, J.-P., and Ceschia, E.: Modelling LAI at a regional scale with ISBA-A-gs: comparison with satellite-derived LAI over southwestern France, Biogeosciences, 6, 1389–1404, doi:10.5194/bg-6-1389-2009, 2009.

Carrer, D., Roujean, J.-L., and Meurey, C.: Comparing Operational MSG/SEVIRI Land Surface Albedo Products From Land SAF With Ground Measurements and MODIS, IEEE T. Geosci. Remote, 48, 1714–1728, doi:10.1109/TGRS.2009.2034530, 2010.

Champeaux, J. L., Masson, V., and Chauvin, F.: ECOCLIMAP: a global database of land surface parameters at 1 km resolution, Meteorol. Appl., 12, 29–32, doi:10.1017/S1350482705001519, 2005.

Cooley, H. S., Riley, W. J., Torn, M. S., and He, Y.: Impact of agricultural practice on regional climate in a coupled land surface mesoscale model, J. Geophys. Res., 110, D03113, doi:10.1029/2004JD005160, 2005.

Courault, D., Seguin, B., and Olioso, A.: Review on estimation of evapotranspiration from remote sensing data: from empirical to numerical modelling approaches, Irrigation and Drainage Systems, 19, 223–249, 2005.

Dorigo, W. A., Zurita-Milla, R., De Wit, A. J. W., Brazile, J., Singh, R., and Schaepman, M. E.: A review on reflective remote sensing and data assimilation techniques for enhanced agroecosystem modeling, Int. J. Appl. Earth Obs., 9, 165–193, 2006.

Edwards, J. M.: Simulation of land surface temperatures: comparison of two climate models and satellite retrievals, Geosci. Model Dev., 2, 123–136, doi:10.5194/gmd-2-123-2009, 2009.

García-Haro, F. J., Camacho-de Coca, F., Meliá, J., and Martínez, B.: Operational derivation of vegetation products in the framework of the LSA SAF project, Proceedings of the EUMETSAT Meteorological Satellite Conference, Dubrovnik (Croatia), 19–23 September 2005a.

García-Haro, F. J., Sommer, S., and Kemper, T.: Variable multiple endmember spectral mixture analysis (VMESMA), Int. J. Remote Sens., 26, 2135–2162, 2005b.

Garrigues, S., Lacaze, R., Baret, F., Morisette, J. T., Weiss, M., Nickeson, J. E., Fernandes, R., Plummer, S., Shabanov, N. V., Myneni, R. B., Knyazikhin, Y., and Yang, W.: Validation and intercomparison of global Leaf Area Index products derived from remote sensing data, J. Geophys. Res., 113, G02028, doi:10.1029/2007JG000635, 2008.

Ge, J.: On the proper use of satellite-derived leaf area index in climate modeling, J. Climate, 22, 4427–4433, doi:10.1175/2009JCLI2868.1, 2009.

Geiger, B., Carrer, D., Franchistéguy, L., Roujean, J.-L., and Meurey, C.: Land Surface Albedo derived on a daily basis from Meteosat Second Generation Observations, IEEE T. Geosci. Remote, 46, 3841–3856, 2008a.

Geiger, B., Meurey, C., Lajas, D., Franchistéguy, L., Carrer, D., and Roujean, J.-L.: Near real time provision of downwelling shortwave radiation estimates derived from satellite observations, Meteorol. Appl., 15, 411–420, 2008b.

Ghent, D., Kaduk, J., Remedois, J., and Balzter, H.: Data assimilation into land surface models: the implications for climate feedbacks, Int. J. Remote Sens., 32, 617–632, doi:10.1080/01431161.2010.517794, 2011.

Gibelin, A.-L., Calvet, J.-C., Roujean, J.-L., Jarlan, L., and Los, S. O.: Ability of the land surface model ISBA-A-gs to simulate leaf area index at the global scale: Comparison with satellites products, J. Geophys. Res., 111, D18102, doi:10.1029/2005JD006691, 2006.

Ghilain, N., Arboleda, A., and Gellens-Meulenberghs, F.: Evapotranspiration modelling at large scale using near-real time MSG SEVIRI derived data, Hydrol. Earth Syst. Sci., 15, 771–786, doi:10.5194/hess-15-771-2011, 2011.

Grippa, M., Kergoat, L., Frappart, F., Araud, Q., Boone, A., de Rosnay, P., Lemoine, J.-M., Gascoin, S., Balsamo, G., Ottle, C., Decharme, B., Saux-Picart, S., and Ramillien, G.: Land water storage variability over West Africa estimated by Gravity Recovery and Climate Experiment (GRACE) and land surface models, Water Resour. Res., 47, W05549, doi:10.1029/2009WR008856, 2011.

Gu, Y., Bélair, S., Mahfouf, J.-F., and Deblonde, G.: Optimal interpolation analysis of leaf area index using MODIS data, Remote Sens. Environ., 104, 283–296, doi:10.1016/j.rse.2006.04.021, 2006.

Ineichen, P., Barroso, C. S., Geiger, B., Hollmann, R., Marsouin, A., and Mueller, R.: Satellite Application Facilities irradiance products: hourly time step comparison and validation over Europe, Int. J. Remote Sens., 30, 5549–5571, doi:10.1080/01431160802680560, 2009.

Jarlan, L., Balsamo, G., Lafont, S., Beljaars, A., Calvet, J.-C., and Mougin, E.: Analysis of leaf area index in the ECMWF land surface model and impact on latent heat and carbon fluxes: Application to West Africa, J. Geophys. Res., 113, D24117, doi:10.1029/2007JD009370, 2008.

Jiang, L., Kogan, F. N., Guo, W., Tarpley, J. D., Mitchell, K. E., Ek, M. B., Tian, Y., Zheng, W., Zou, C.-Z., and Ramsay, B. H.: Real-time weekly global green vegetation fraction derived from advanced very high resolution radiometer-based NOAA operational global vegetation index (GVI) system, J. Geophys. Res., 115, D11114, doi:10.1029/2009JD013204, 2010.

Jimenez, M. A., Mira, A., Cuxart, J., Luque, A., Alonso, S., and Guijarro, J. A.: Verification of a Clear-Sky Mesoscale Simulation Using Satellite-Derived Surface Temperatures, Mon. Weather Rev., 136, 5148–5161, 2008.

Joffre, R., Rambal, S., and Romane, F.: Local variations of ecosystem functions in a Mediterranean evergreen oak woodland, Ann. For. Sci., 53, 561–570, 1996.

Jung, M., Henkel, K., Herold, M., and Churkina, G.: Exploiting synergies of global land cover products for carbon cycle modeling, Remote Sens. Environ., 101, 534–553, doi:10.1016/j.rse.2006.01.020, 2006.

Kahan, D. S., Xue, Y., and Allen, S. J.: The impact of vegetation and soil parameters in simulations of surface energy and water balance in the semi-arid sahel: A case study using SEBEX and HAPEX-Sahel data, J. Hydrol., 320, 238–259, doi:10.1016/j.jhydrol.2005.07.011, 2006.

Kalma, J. D., McVicar, T. R., and McCabe, M. F.: Estimating Land Surface Evapotranspiration: A Review of Methods Using Remotely Sensed Surface Temperature Data, Surv. Geophys., 29, 421–469, doi:10.1007/s10712-008-9037-z, 2008.

Kaptué Tchuente, A. T., Roujean, J.-L., and Faroux, S.: ECOCLIMAP-II: an ecosystem classification and land surface parameter database of Western Africa at 1 km resolution for the African Monsoon Multidisciplinary Analysis (AMMA) project, Remote Sens. Environ., 114, 961–976, 2010.

Kato, H., Rodell, M., Beyrich, F., Cleugh, H., van Gorsel, E., Liu, H., and Meyers, T. P.: Sensitivity of Land Surface Simulations to Model Physics, Parameters, and Forcings, at Four CEOP Sites, J. Meteor. Soc. Jpn., 85A, 187–204, 2007.

Kergoat, L., Grippa, M., Baille, A., Lacaze, R., Mougin, E., Ottlé, C., Pellarin, T., Polcher, J., de Rosnay, P., Roujean, J.-L., Sandholt, I., Taylor, C. M., Zin, I., and Zribi, M.: Remote sensing of the land surface during the African Monsoon Multidisciplinary Analysis (AMMA), Atmospheric Science Letters, Special Issue: African Monsoon Multidisciplinary Analysis (AMMA): an integrated project for understanding of the West African climate system and its human dimension, Atmos. Sci. Lett., 12, 129–134, doi:10.1002/asl.325, 2011.

Kutsch, W. L., Hanan, N., Scholes, B., McHugh, I., Kubheka, W., Eckhardt, H., and Williams, C.: Response of carbon fluxes to water relations in a savanna ecosystem in South Africa, Biogeosciences, 5, 1797–1808, doi:10.5194/bg-5-1797-2008, 2008.

LSA-SAF VEGA Team – Camacho-de-Coca, F., Garcia-Haro, F. J., Verger, A., and Melia, J.: LSA-SAF Product User Manual: Vegetation parameters (FVC, LAI, FAPAR), PUM-VEGAv2.1, 2008.

Li, Z.-L., Tang, R., Wan, Z., Bi, Y., Zhou, C., Tang, B., Yan, G., and Zhang, X.: A review of current methodologies for regional evapotranspiration estimation from remotely sensed data, Sensors, 9, 3801–3853, doi:10.3390/s90503801, 2009.

Masson, V., Champeaux, J. L., Chauvin, F., Meriguet, Ch., and Lacaze, R. A.: Global database of land surface parameters at 1-km resolution in meteorological and climate models, J. Climate, 16, 1261–1282, 2003.

Merbold, L., Ardö, J., Arneth, A., Scholes, R. J., Nouvellon, Y., de Grandcourt, A., Archibald, S., Bonnefond, J. M., Boulain, N., Brueggemann, N., Bruemmer, C., Cappelaere, B., Ceschia, E., El-Khidir, H. A. M., El-Tahir, B. A., Falk, U., Lloyd, J., Kergoat, L., Le Dantec, V., Mougin, E., Muchinda, M., Mukelabai, M. M., Ramier, D., Roupsard, O., Timouk, F., Veenendaal, E. M., and Kutsch, W. L.: Precipitation as driver of carbon fluxes in 11 African ecosystems, Biogeosciences, 6, 1027–1041, doi:10.5194/bg-6-1027-2009, 2009.

Miller, J., Barlage, M., Zeng, X., Wei, H., Mitchell, K., and Tarpley, D.: Sensitivity of the NCEP/Noah land surface model to the MODIS green vegetation fraction data set, Geophys. Res. Lett., 33, L13404, doi:10.1029/2006GL026636, 2006.

Nash, J. E. and Suttcliffe, J. V.: River Flow Forecasting through Conceptual Models, Part I-A Discussion of Principles, J. Hydrol., 10, 282–290, 1970.

Noilhan, J. and Planton, S.: A simple parameterization of land surface processes for meteorological models, Mon. Weather Rev., 117, 536–549, 1989.

Oleson, K. and Bonan, G.: The effects of remotely sensed plant functional type and leaf area index on simulations of boreal forest surface fluxes by the NCAR land surface model, J. Hydrometeorol., 1, 431–446, 2000.

Pekel, J. F., Bartholomé, E., and Clerici, M.: Assessing the use of LSA-SAF VEGA data for environmental monitoring in Africa: fractional cover and natural vegetation condition assessment, LSA-SAF 4th user workshop, Toulouse 16 April 2010, available at: http://landsaf.meteo.pt (last access: 2 August 2012), 2010.

Pereira, J. S., Mateus, J. A., Aires, L. M., Pita, G., Pio, C., David, J. S., Andrade, V., Banza, J., David, T. S., Paço, T. A., and Rodrigues, A.: Net ecosystem carbon exchange in three contrasting Mediterranean ecosystems – the effect of drought, Biogeosciences, 4, 791–802, doi:10.5194/bg-4-791-2007, 2007.

Rebmann, C., Zeri, M., Lasslop, G., Mund, M., Kolle, O., Schulze, E.-D., and Feigenwinter, C.: Treatment and assessment of the CO2-exchange at a complex forest site in Thuringia, Germany, Agr. Forest Meteorol., 150, 684–691, 2010.

Rodell, M., Houser, P. R., Jambor, U., Gottschalck, J., Mitchell, K., Meng, C.-J., Arsenault, K., Cosgrove, B., Radakovich, J., Bosilovich, M., Entin, J. K., Walker, J. P., Lohmann, D., and Toll, D.: The Global Land Data Assimilation System, B. Am. Meteorol. Soc., 85, 381–394, 2004.

Sepulcre-Cantó, G., Gellens-Meulenberghs, F., Arboleda, A., Duveiller, G., De Wit, A., Eerens, H., Djaby, B., and Defourny, P.: Estimating crop specific evapotranspiration using remote sensing imagery at various spatial resolutions for improving crop growth modeling, Int. J. Remote Sens., in press, 2012.

Simmons, A., Uppala, S., Dee, D., and Kobayashi, S.: ERA-Interim: New ECMWF reanalysis products from 1989 onwards, ECMWF Newsletter, 10, 26–35, 2006.

Sjöström, M., Ardö, J., Eklundh, L., El-Tahir, B. A., El-Khidir, H. A. M., Hellström, M., Pilesjö, P., and Seaquist, J.: Evaluation of satellite based indices for gross primary production estimates in a sparse savanna in the Sudan, Biogeosciences, 6, 129–138, doi:10.5194/bg-6-129-2009, 2009.

Stisen, S., Sandholt, I., Noergaard, A., Fensholt, R., and Jensen, K. H.: Combining the triangle method with thermal inertia to estimate regional evapotranspiration – Applied to MSG-SEVIRI data in the Senegal River basin, Remote Sens. Environ., 110, 1242–1255, doi:10.1016/j.rse.2007.08.013, 2008.

Suni, T., Berninger, F., Vesala, T., Markkanen, T., Pertti, H., Makela, A., Ilvesniemi, H., Hanninen, H., Nikinmaa, E., Huttula, T., Laurila, T., Aurela, M., Grelle, A., Lindroth, A., Arneth, A., Shibistova, O., and Lloyd, J.: Air temperature triggers the recovery of evergreen boreal forest photosynthesis in spring, Global Change Biol., 9, 1410–1426, doi:10.1046/j.1365-2486.2003.00597.x, 2003.

Tian, Y., Dickinson, R. E., Zhou, L., Zeng, X., Dai, Y., Myneni, R. B., Knyazikhin Y., Zhang, X., Friedl, M., Yu, H., Wu, W., and Shaick, M.: Comparison of seasonal and spatial variations of LAI and fraction of absorbed photosynthetically active radiation from Moderate Resolution Imaging Spectroradiometer (MODIS) and Common Land Model, J. Geophys. Res., 109, D01103, doi:10.1029/2003JD003777, 2006.

Trigo, I. F., Monteiro, I. T., Olesen, F., and Kabsch, E.: An assessment of remotely sensed land surface temperature, J. Geophys. Res., 113, D17108, doi:10.1029/2008JD010035, 2008.

Trigo, I. F., DaCamara, C. C., Viterbo, P., Roujean, J.-L., Olesen, F., Barroso, C., Camacho-de Coca, F., Carrer, D., Freitas, S. C., Garcia-Haro, J., Geiger, B., Gellens-Meulenberghs, F., Ghilain, N., Melia, J., Pessanha, L., Siljamo, N., and Arboleda, A.: The Satellite Application Facility on Land Surface Analysis, Int. J. Remote Sens., 32, 2725–2744, doi:10.1080/01431161003743199, 2011.

van den Hurk, B. J. J. M., Viterbo, P., Beljaars, A. C. M., and Betts, A. K.: Offline validation of the ERA40 surface scheme, ECMWF Technical Memorandum, 295, 41 pp., 2000.

van den Hurk, B. J. J. M., Viterbo, P., and Los, S.: Impact of leaf area index seasonality on the annual land surface evaporation in a global circulation model, J. Geophys. Res., 108, 4191, doi:10.1029/2002JD002846, 2003.

Verger, A., Camacho, F., García-Haro, F. J., and Meliá, J.: Prototyping of Land-SAF leaf area index algorithm with VEGETATION and MODIS data over Europe, Remote Sens. Environ., 113, 2285–2297, doi:10.1016/j.rse.2009.06.009, 2009.

Viterbo, P. and Beljaars, A. C. M.: An improved land surface parameterization scheme in the ECMWF model and its validation, J. Climate, 8, 2716–2748, 1995.

Williams, M., Richardson, A. D., Reichstein, M., Stoy, P. C., Peylin, P., Verbeeck, H., Carvalhais, N., Jung, M., Hollinger, D. Y., Kattge, J., Leuning, R., Luo, Y., Tomelleri, E., Trudinger, C. M., and Wang, Y.-P.: Improving land surface models with FLUXNET data, Biogeosciences, 6, 1341–1359, doi:10.5194/bg-6-1341-2009, 2009.

Wipfler, E. L., Metselaar, K., van Dam, J. C., Feddes, R. A., van Meijgaard, E., van Ulft, L. H., van den Hurk, B., Zwart, S. J., and

Bastiaanssen, W. G. M.: Seasonal evaluation of the land surface scheme HTESSEL against remote sensing derived energy fluxes of the Transdanubian region in Hungary, Hydrol. Earth Syst. Sci., 15, 1257–1271, doi:10.5194/hess-15-1257-2011, 2011.

Yang, W., Huang, D., Tan, B., Stroeve, J. C., Shabanov, N. V., Knyazikhin, Y., Nemani, R. R., and Myneni, R. B.: Analysis of leaf area index and fraction of PAR absorbed by vegetation products from the Terra MODIS sensor: 2000–2005, IEEE Trans. Geosci., 44, 1829–1842, doi:10.1109/TGRS.2006.871214, 2006a.

Yang, W., Shabanov, N. V., Huang, D., Wang, W., Dickinson, R. E., Nemani, R. R., Knyazikhin, Y., and Myneni, R. B.: Analysis of leaf area index products from combination of MODIS Terra and Aqua data, Remote Sens. Environ., 104, 297–312, doi:10.1016/j.rse.2006.04.016, 2006b.